ARTICLE

DOI: 10.1590/2317-4889201920190067

BJGEO
Brazilian Journal of Geology

U-Pb SHRIMP dating of basement rocks of the Iriri-Xingu domain, Central Amazonian province, Amazonian craton, Brazil

Marcelo Lacerda Vasquez[1]*, Umberto Giuseppe Cordani[2], Kei Sato[2], Jaime dos Passos de Oliveira Barbosa[1], Maria Telma Lins Faraco[1], Victor Câmara Maurer[3]

Abstract

The Iriri-Xingu domain, located in the central part of the Amazonian craton, consists of extensive occurrences of Paleoproterozoic volcanic rocks and granites with published ages of ca. 1990 to 1840 Ma, which show a strong crustal contribution for their magmas. Exposures of basement rocks are small and rare. Samples from two areas were dated in this work by U-Pb SHRIMP in zircon. In the northern Maribel area, a high-grade pelitic paragneiss presented an age of 2160 ± 8 Ma and the leucosome of a migmatitic orthogneiss, probably a diatexite, crystallized at 2149 ± 20 Ma. These Rhyacian ages suggest that it is part of the Bacajá domain, related to the Trans-Amazonian cycle. The Morro Grande area occurs in the central part of Iriri-Xingu domain, where a high-grade muscovite gneiss with a protolith of 2120–2180 Ma is dated at 1982 ± 7 Ma, and the leucosome of a migmatitic orthogneiss is crystallized at 1979 ± 8 Ma. These are the first records of high-grade metamorphism at ca. 1980 Ma in the Central Brazil shield and may be related to the generation of this Orosirian felsic magmatism, which is widespread throughout the nearby Ventuari-Tapajós province.

KEYWORDS: U-Pb geochronology; sensitive high-resolution ion microprobe (SHRIMP); Iriri-Xungu domain; Amazonian craton.

INTRODUCTION

The Central Amazonian province of the Amazonian craton was originally defined by Cordani *et al.* (1979). Their paper was the first in which the tectonic evolution of the Amazonian craton was considered by means of a mobilistic approach and was characterized as a stable area in relation to the Paleoproterozoic Maroni-Itacaiunas mobile belt to the northeast. The tectonically stabilized Archean nucleus of Carajás region is included in its southeastern part, and its volcanic-sedimentary cover rocks characterize the cratonic nature of the province. The initial work of Cordani *et al.* (1979) was followed and upgraded by many others, such as Cordani and Teixeira (2007) and Tassinari and Macambira (1999), from which Figure 1 has been adapted. Regarding the Central Amazonian province, Tassinari and Macambira (1999, 2004) distinguished the Archean Carajás block from Xingu-Iricoumé block, which includes large outcrops of Paleoproterozoic felsic volcanic rocks and granites. Based on the Nd isotopic data presented by Sato and Tassinari (1997), the existence of Archean crustal sources for these igneous rocks was proposed, which contrasted with the juvenile sources of coeval igneous rocks occurring within the adjacent Ventuari-Tapajós province to the west.

The Iriri-Xingu domain (IXD) comprises large outcrops of Paleoproterozoic felsic volcanic rocks and granites in the southern part of Central Amazonian province (Fig. 1). Direct exposure of dated Archean basement below rocks of the IXD has not been encountered yet. Currently, the only confirmed Archean part of the Central Amazonian province is Carajás block (Cordani *et al.* 1984, Tassinari and Macambira 1999, 2004).

The regional geology around the IXD is divided into seven tectonic domains characterized by coherence in terms of lithostratigraphy, geochronology, structural trends, and geophysical features (Vasquez *et al.* 2008b, Fig. 1):

- Rio Maria domain (RMD) – exposed Mesoarchean (3050–2850 Ma) terrains at the southeastern corner of the Central Amazonian province;
- Carajás domain (CJD) – exposed Neoarchean terrains (2760–2570 Ma) at the southeastern corner of the Central Amazonian province;
- Bacajá domain (BJD) – Mesoarchean to Siderian (3000–2300 Ma) terrains reworked during the Rhyacian orogenies of the Transamazonian cycle (2260–2050 Ma), at the southeastern corner of Maroni-Itacaiúnas province;
- Santana do Araguaia domain (SAD) – Neoarchean and Mesoarchean terrains reworked in Paleoproterozoic time with local reworking by the Transamazonian cycle;
- IXD – Orosirian volcanic-plutonic igneous rocks of different types overlying the basement of Central Amazonian province, with ages between 1990 and 1840 Ma;

[1]Serviço Geológico do Brasil – Belém (PA), Brazil.
E-mails: marcelo.vasquez@cprm.gov.br; jaime.barbosa@cprm.gov.br; telmafaraco@yahoo.com.br

[2]Instituto de Geociências, Universidade de São Paulo – São Paulo (SP), Brazil. E-mails: ucordani@usp.br; keisato@usp.br

[3]Escola de Minas, Universidade Federal de Ouro Preto – Ouro Preto (MG), Brazil. E-mail: camaramaurer@gmail.com

*Corresponding author.

- Tapajós domain (TJD) – Orosirian volcanic-plutonic igneous rocks, orthogneisses and supracrustal rocks of Ventuari-Tapajós province, some with of juvenile character;
- Juruena domain (JRD) – Orosirian to Statherian volcanic-plutonic igneous rocks (1820–1770 Ma), which overly rocks of the IXD and TJD.

The IXD is formed by I- and A-type felsic volcanic rocks and granites emplaced in two main pulses: 1990–1970 Ma and 1890–1840 Ma. Based on Nd isotopic data for rocks of the younger pulse, Sato and Tassinari (1997) identified Archean crustal sources for these parent magmas, with strongly negative ε_{Nd} (-5.4 to -12.1) and Mesoarchean to Neoarchean T_{DM} model ages (3.3 to 2.6 Ga). Their measurements contrasted with the mainly juvenile Nd isotope signature of rocks from the TJD in the adjacent Paleoproterozoic Ventuari-Tapajós tectonic province to the west, which forms at least part of the IXD basement.

Based on such considerations, it becomes important to examine all areas in which confirmed basement of the IXD is exposed. A previous geological survey in the 1970s (SUDAM, Geomitec 1972) mapped only small outcrops of metamorphic rocks in the western part of the IXD (Morro Grande area), and Vasquez *et al.* (2008b) mapped another in the northeastern part (Maribel area). These two localities are indicated in Figure 2. In this paper, we present zircon U-Pb ages and discuss their bearing on tectonic evolution of the IXD and of the entire Amazonian craton.

GEOLOGY OF THE IRIRI-XINGU DOMAIN

Orthogneisses, migmatites, and foliated granitoids were mapped in the southeastern part of the study region (Fig. 2). Their protolith was formed around 2830 Ma (Tab. 1), probably by juvenile accretion of calc-alkaline magmas related to

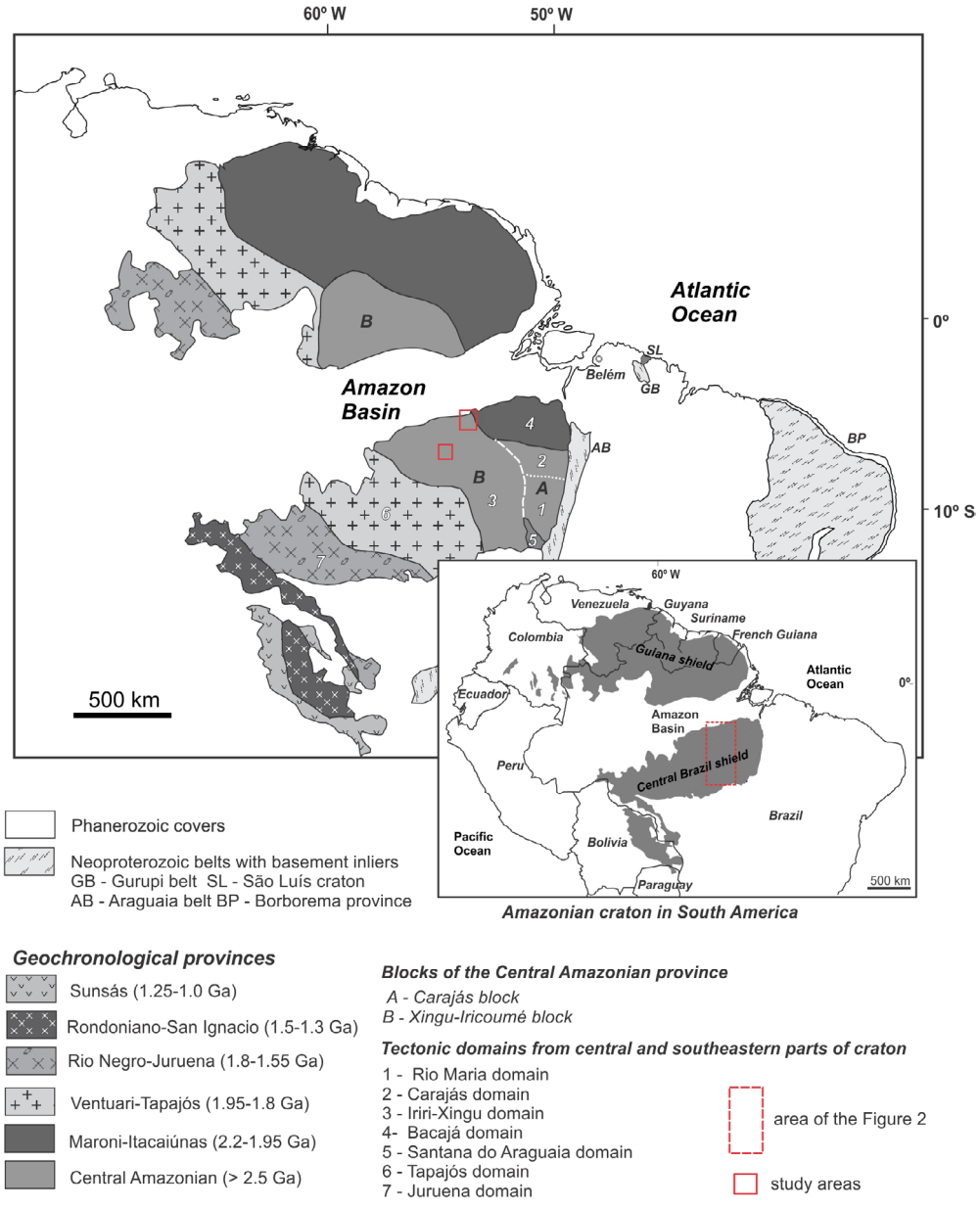

Figure 1. Sketch map of geochronological provinces from the Amazonian craton based on Tassinari and Macambira (2004), with location of the tectonic domains of Vasquez *et al.* (2008b).

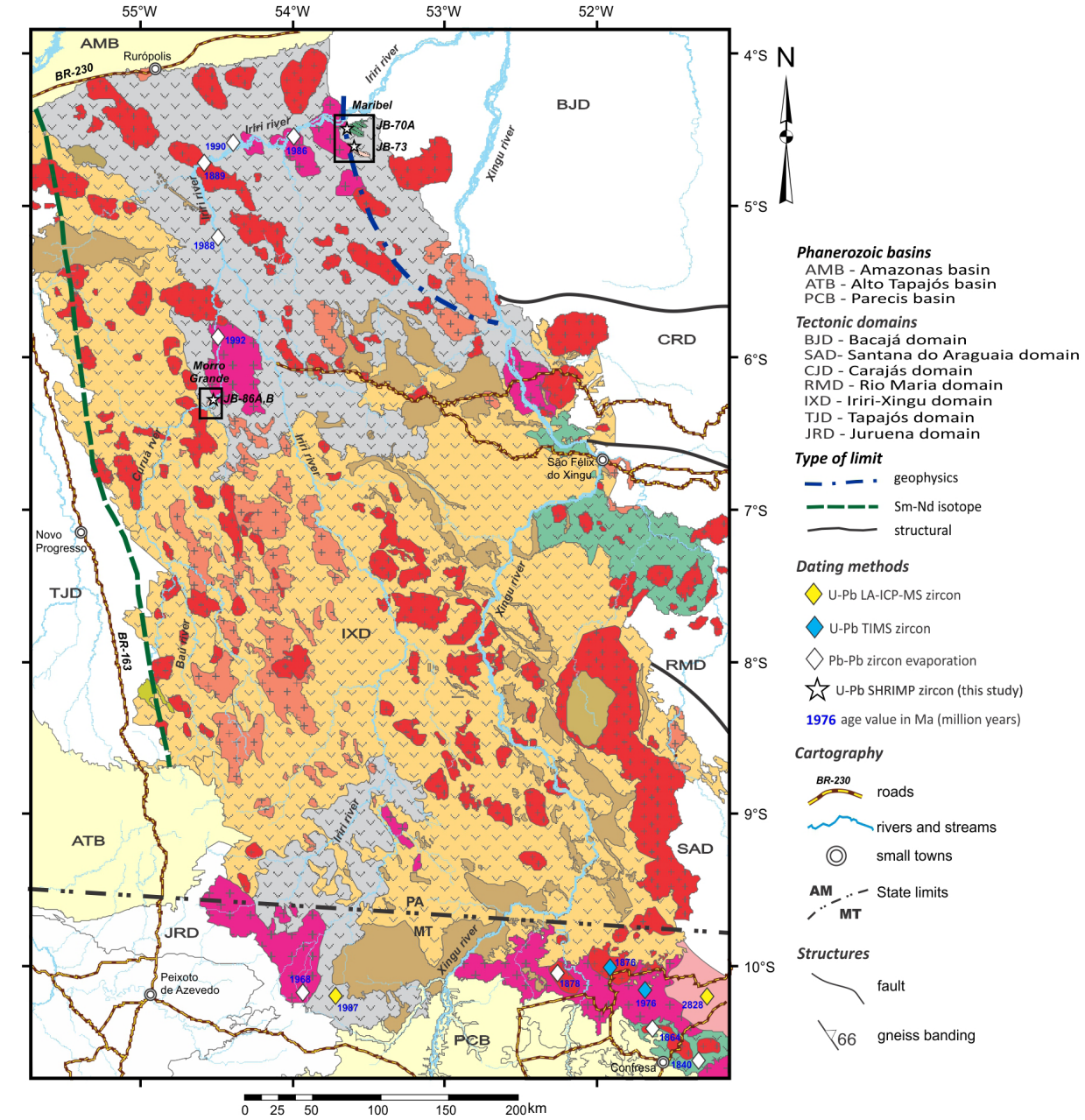

Phanerozoic sedimentary basin and alluvial deposits.

Paleoproterozoic Sedimentary Basins

Quartz rich-, lithic and arkose sandstones, red mudstones and polymitic conglomerate (volcanic and pyroclastic rocks boulders) with local ash-tuffs and cherts. An epiclastic continetal basin post-Orosirian volcanisms. Triunfo (< 1860 Ma) and Cubencranquém (< 1840 Ma) Formations.

Metasandstones (quartz-arenites) and metaconglomerates (quatz and supracrustal rocks boulders). A continental rift basin that underwent open folding and low-grade metamorphism. Castelo dos Sonhos Formation (2050 - 2011 Ma).

Paleoproterozoic Vulcano-plutonisms

Syenogranites, K-feldspar granites and quartz syenites. Alkaline granites (A-type) with Meso- to Neoarchean magmas sources. Rio Dourado (1884 - 1864 Ma), Velho Guilherme (1867 - 1862 Ma) Suite , Serra Queimada Granite (1882 Ma) and A-type granites of W- and N-part domain (1889 Ma).

Monzogranites, quartz monzonites and granodiorites. High-K calc-alkaline (I-type) granitoids that are coeval with A-type granites of *ca.* 1880 Ma.

Andesites, latites, lati-andesites, quartz latite and dacites, lava and ignimbrite flows, with pyroclastic and volcanolcastic rocks associated. High-K calc-alkaline rocks with Mesoarchean to Siderian magmas sources. Sobreiro Formation (1880 - 1865 Ma) and Confresa Dacite (1840 Ma) .

Rhyolites, alkali rhyolites and rhyodacites, lava and ignimbrite flows with porphyry microgranites, pyroclastic and volcanolcastic rocks assciated. Alkaline saturated (A-type) volcanic rocks with Neoarchean magmas sources. Santa Rosa Formation (1888 - 1879 Ma) .

Syenogranites to tonalites and quartz monzonites to diorites, local prothomylonites. High-K calc-alkaline granitoids with Neoarchean to Siderian magmas sources. Vila Rica Suite (1976 - 1968 Ma) and I-type granites of W- and N-parts of domain (1992 - 1986 Ma).

Dacites to rhyolites, lava and pyroclastic flows, with volcanolcastic rocks. High-K calc-alkaline rocks with Neoarchean magmas sources. Iriri (1990 - 1988 Ma) and Jarinã (1987 Ma) Formartions.

Basement Rocks

Mafic schists, mica schists, quartzites and pelitic paragneiss of Maribel area.

Migmatic ortogneiss of Maribel area.

Muscovite gneiss of Morro Grande area.

Migmatitic orthogneiss of Morro Grande area.

Tonalitic to granitic orthogneisses, migmatites, porphyroclastic and banded granites. Ortogneisses with protholith of 2828 Ma in SE-part and 2503 - 2487 Ma in NE-part (Figure 3).

Figure 2. Geological map of the Iriri-Xingu domain with previous geochronological data and location of the study areas and dated samples (modified after Vasquez *et al.* 2008b). Detailed geological maps of (A) Maribel and (B) Morro Grande areas.

an island arc (Alves *et al.* 2010). These basement rocks were related to the SAD (Alves *et al.* 2010), but their high-grade metamorphism was not dated to test for reworking during the Rhyacian Trans-Amazonian cycle. Therefore, these high-grade metamorphic rocks might be part of the IXD.

Felsic volcanic and pyroclastic rocks are dominant in the IXD (Fig. 2), but zircon ages have shown an association with different volcanic-plutonic events (Tab. 1). In the original proposal (SUDAM, Geomitec 1972), they were named Iriri Formation, but Silva *et al.* (1974) revised, changed it to Iriri Group, and individualized some andesites and dacites as the Sobreiro Formation. These felsic rocks have been related to the Uatumã magmatism (Macambira and Vale 1997, Teixeira *et al.* 2002), which represents the main Paleoproterozoic volcanic-plutonic event of the Amazonian craton at ca. 1880 Ma (Dall'Agnol *et al.* 1994). Zircon ages between 1888 and 1879 Ma (Tab. 1) were obtained on volcanic lavas and pyroclastic rocks, as well as microgranites related to the eastern part of the domain (Santa Rosa Formation), which confirm such correlation. However, the volcanic rocks from the northern and western parts of the IXD (Fig. 2) are composed of dacites, rhyolites, and felsic ignimbrites extruded between 1990 and 1986 Ma (Tab. 1). In the southern part of the domain, Alves *et al.* (2010) mapped high-K calc-alkaline quartz latitic to rhyolitic lavas and ignimbrites of 1987 Ma (Jarinã Formation). They show that volcanism of this age is also widespread in the IXD. The youngest dated felsic rock is a dacite at 1840 Ma (Tab. 1) associated with pyroclastic and volcanogenic sedimentary rocks in the southeastern part of the domain.

Fernandes *et al.* (2011) identified A-type geochemistry for the rhyolitic rocks of the Santa Rosa Formation and I-type high-K calc-alkaline geochemistry for the andesitic rocks of Sobreiro Formation. Based on trace elements and Nd isotope data, they proposed that the Sobreiro Formation magma was formed by mixing mantle-derived and anatectic melts of Archean age, but A-type magmas of Santa Rosa Formation were a result from anatexis of different Archean crust sources (3.0 to 2.5 Ga).

Vasquez *et al.* (2008b) mapped several plutons of I- and A-type granites in the western and northern parts of the IXD (Fig. 2). Semblano *et al.* (2016) obtained zircon ages of 1992 and 1986 Ma for two I-type granites, and an age of 1889 Ma for an A-type granite (Tab. 1). Alves *et al.* (2010) mapped high-K calc-alkaline granites of the Vila Rica Suite (dated at 1976 and 1968 Ma) in the southeastern part of the domain. Moreover,

Table 1. Summary of geochronological data of the Iriri-Xingu domain.

Lithostratigraphic unit	Age formation (Ma)	Method	Ref.	TDM (Ga)	ε Nd (t)	Ref.
N- and W-part						
A-type granites	1889 ± 2	Pb-Pb E zr	Semblano *et al.* (2016)	2.87	-8.76	Sato and Tassinari (1997)
			Semblano *et al.* (2016)	2.55	-5.35	Sato and Tassinari (1997)
I-type granites	1992 ± 3/1986 ± 4	Pb-Pb E zr	Semblano *et al.* (2016)	2.43/2.60	-2,82/-5.29	Semblano *et al.* (2016)
Iriri Formation	1990 ± 4/1988 ± 2	Pb-Pb E zr	Semblano *et al.* (2016)	2.57/2.61/3.13	-4.17/-5.38 /-9.95	Semblano *et al.* (2016)
E-part						
Velho Guilherme Suite	1862 ± 3/1866 ± 3/1867 ± 4	Pb-Pb E zr	Teixeira *et al.* (2002)			
Serra Queimada Granite	1882 ± 12	Pb-Pb E zr	Pinho *et al.* (2006)			
Sobreiro Formation	1865 ± 5	Pb-Pb E zr	Teixeira *et al.* (2002)	3.11	-10.1	Teixeira *et al.* (2002)
	1880 ± 6	Pb-Pb E zr	Pinho *et al.* (2006)	2.49 to 2.89	-4.56 to -9.61	Fernandes *et al.* (2011)
Santa Rosa Formation	1884 ± 2, 1879 ± 2	Pb-Pb E zr	Juliani and Fernandes (2010)	2.56 to 3.12	-5.80 to -11.39	Fernandes *et al.* (2011)
	1888 ± 3/1887 ± 2/1881 ± 3/1881 ± 2	Pb-Pb E zr	Pinho *et al.* (2006)			
S- and SE-part						
Confresa Dacite	1840 ± 8	U-Pb T zr	Alves *et al.* (2010)	2.47	-4.06	Alves *et al.* (2010)
Rio Dourado Suite	1876 ± 11	U-Pb T zr	Barros *et al.* (2011)	2.62/2.61/3.10	-3.10/-10.7/-7.81	Barros *et al.* (2011)
	1878 ± 4, 1864 ± 5	Pb-Pb E zr	Alves *et al.* (2010)	2.7	-7.09	Alves *et al.* (2010)
	1884 ± 4	U-Pb T zr	Barros *et al.* (2006)			
Vila Rica Suite	1976 ± 9	U-Pb T zr	Padilha (2007)	2.66	-5.96	Padilha (2007)
	1968 ± 2	Pb-Pb E zr	Alves *et al.* (2010)	2.74	-7.3	Alves *et al.* (2010)
Jarinã Formation	1987 ± 14	U-Pb L zr	Alves *et al.* (2010)	2.55/2.57	-4.59/-5.40	Alves *et al.* (2010)
Santana do Aragauaia Complex	2828 ± 21	U-Pb T zr	Alves *et al.* (2010)	2.89/2.84	1.09/1.83	Alves *et al.* (2010)

E: Pb-evaporation; S: SHRIMP; T: ID-TIMS; L: LA-ICP-MS; zr: zircon.

Macambira and Vale (1997) obtained a Rb-Sr isochron age of 1921 ± 69 Ma for one I-type granite of São Felix do Xingu area and suggested that such plutonic event also occurred in the eastern part of the IXD, which is dominantly composed by A-type granites of 1882 to 1862 Ma (Tab. 1).

Sm-Nd isotopic data (Tab. 1) show that Archean material was the main source of magma for the Orosirian igneous rocks. However, a weak negative ε_{Nd} (-2.8) and Siderian T_{DM} model age (2.4 Ga) of one I-type granite of the western part of the domain suggests mixing of Archean crustal with Paleoproterozoic juvenile material (Semblano *et al*. 2016). This juvenile source is stronger in the continuation of the Central Amazonian province in the Guiana shield, as shown in the ε_{Nd} -3.0 to 2.9 and T_{DM} 2.39 to 1.95 Ga of igneous rocks of 1.99-1.98 Ga and 1.89-1.88 Ga (Barreto *et al*. 2014, Leal *et al*. 2018). Based on Nd isotope data and absence of Archean heritage, Barreto *et al*. (2014) have supported a discussion on the occurrence of the Central Amazonian province in this shield and the east limit of Ventuari-Tapajós province.

Most of the Paleoproterozoic sedimentary basins of the IXD are younger than the Orosirian volcanic rocks (Fig. 2). Only in the southwestern part, there is an older sedimentary basin (Castelo dos Sonhos Formation) formed between 2050 and 2011 Ma (Klein *et al*. 2016). Metasandstones and meta-conglomerates of this basin represent alluvial fans and braided fluvial sediments, which underwent open folding, local ductile deformation, and low-grade metamorphism. Vasquez *et al*. (2008b) considered this basin as part of the IXD, but Klein *et al*. (2016) relate it to a continental rift system in the early stages of Tapajós domain.

Post-volcanism sedimentary basins (Triunfo and Cubencranquém formations) are composed of quartz-rich sandstones, lithic and arkosic sandstones, red mudstones and polymict conglomerates with volcanic and pyroclastic rocks boulders (Macambira and Vale 1997, Alves *et al*. 2010). The distal fallout pyroclastic material is represented by local ash-tuffs, and chert layers are considered as chemical sediments related to volcanic processes coeval with epiclastic sedimentation.

GEOCHRONOLOGY

Sampling locations and analytical methods

Two areas were selected to study the basement rocks of the IXD: Maribel in the northeast, close to the border with the Bacajá Domain, and Morro Grande in the west (Fig. 2). Two types of samples from each area were selected for geochronological work. A pelitic paragneiss and a migmatitic orthogneiss from Maribel and a muscovite gneiss and a migmatitic orthogneiss from Morro Grande.

For each sample, U-Pb SHRIMP determinations on single zircon crystals were carried out, employing the sensitive high-resolution ion microprobe (SHRIMP II) at Universidade de São Paulo (USP). The selected zircon grains were mounted in epoxy resin together with standard fragments, and the mounts were covered by a thin layer of gold (6-8 ηm) to assure uniform electrical conductivity. Scanning electron microscopy (SEM) was applied to produce cathodoluminescence (CL) images before the SHRIMP work, in order to select the best zircon domains for the analyses. The high-resolution CL images of

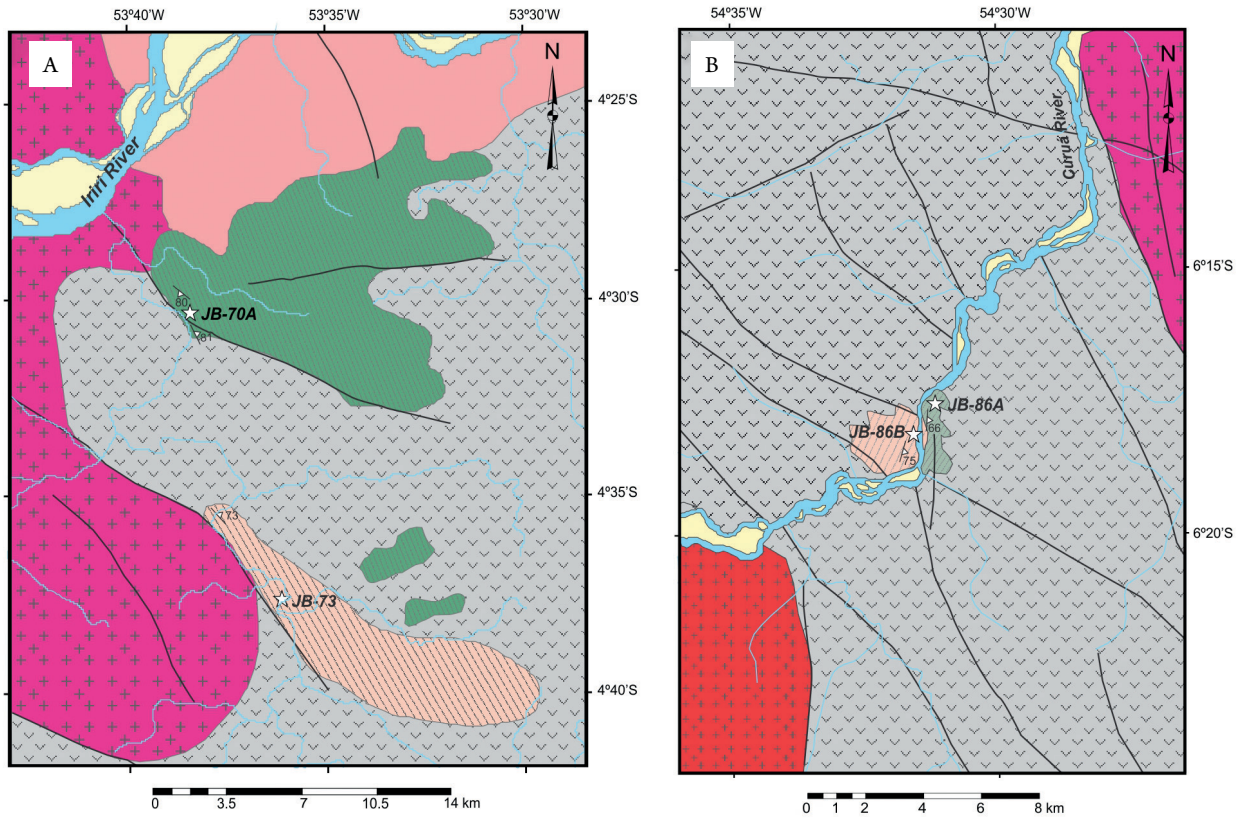

Figure 3. Geological maps of (A) Maribel and (B) Morro Grande areas. Subtitles of geological units and structures are in Figure 2.

zircon crystals were undertaken in the SEM laboratory of the branch office of CPRM Belém (LAMIN-BE).

Details of the SHRIMP analytical procedures, including calibration methods, were presented by Williams (1998), and the work at the São Paulo laboratory was described by Sato *et al.* (2014). Uranium abundance and U/Pb ratios were calibrated against the Z6266 (903 ppm, Stern and Ameling 2003) and Temora 2 (416.78 Ma, Black *et al.* 2004) standards, respectively, and the individual ages were determined from five successive scans of the mass spectrum.

Age values in tables and figures are given with 2s precision, and the average ages reported in the text are weighted mean $^{207}Pb/^{206}Pb$ ages with 95% confidence limits. Correction for common Pb was made based on the measured ^{204}Pb, and the typical error component for the $^{206}Pb/^{238}U$ ratios was less than 2%. Data were reduced by using SQUID software (Ludwig 2009a), and the Concordia diagrams and cumulative Gaussian plots were prepared using Isoplot/Ex (Ludwig 2009b).

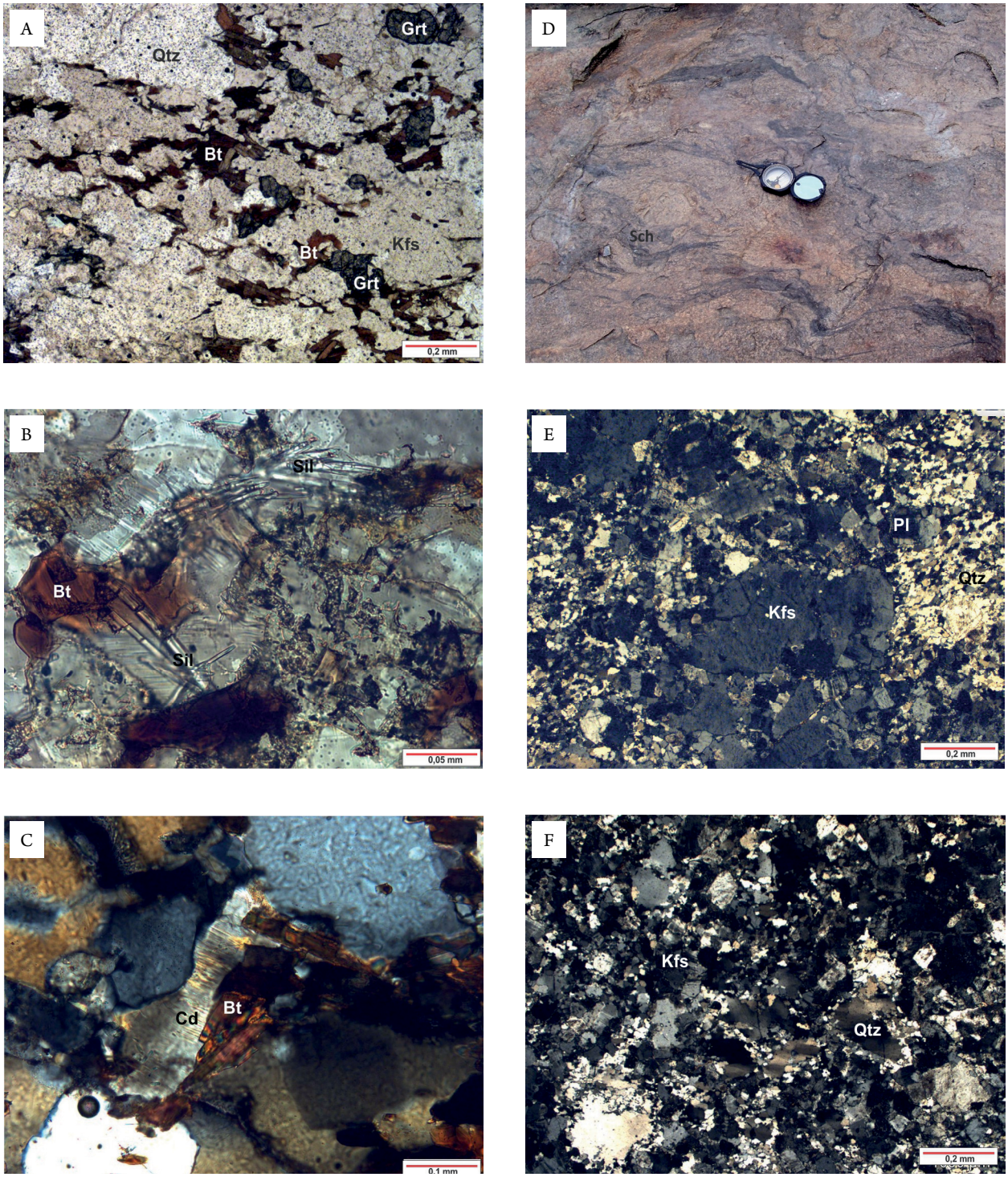

Figure 4. Basement rocks of Maribel area: JB-70A pelitic paragneiss sample: (A and B): plane polarized light; (C) crossed polarized light; (A) Granolepidoblastic texture with quartz (Qtz), K-feldspar (Kfs), porphyroblasts of garnet (Grt) and biotite (Bt); (B) Sillimanite (Sil) fibrous crystal and biotite; (C) Cordierite (cd) and biotite. JB-73 migmatitic orthogneiss sample: (D) Schlieren (Sch) and banding; (E and F) crossed polarized light; (E) Porphyroclast of K-feldspar (Kfs), recrystallized quartz (Qtz) grain in a granoblastic matrix and relicts of zoned plagioclase (Pl); (F) Core-and-mantle (mortar) texture in porphyroclasts of quartz (Qtz) and K-feldspar (Kfs) with mechanically crushed and sub-grain mantles.

Sample descriptions and respective U-Pb zircon ages

In the Maribel area, the high-K calc-alkaline volcanic rocks of ca. 1990 Ma cover an area of supracrustal rocks, pelitic paragneisses, as well as migmatitic orthogneiss (Fig. 3A). The small body (< 2 km²) of Morro Grande, located in the western part of the IXD (Fig. 2), includes a migmatitic orthogneiss and a muscovite gneiss. It is surrounded by felsic volcanic rocks and granitoids of ca. 1990 Ma (Fig. 3B).

Pelitic paragneiss JB-70A

This pelitic paragneiss from Maribel exhibits banding with granolepidoblastic texture and comprises garnet porphyroblasts (Fig. 4A), flakes of red biotite (high-Ti), sillimanite (Fig. 4B) and cordierite (Fig. 4C). This paragneiss was formed in high-grade conditions that correspond to upper amphibolite facies, according to mineral assemblages (Pattison *et al.* 2003, Bucher and Grapes 2011).

One population of zircon grains provided near concordant $^{207}Pb/^{206}Pb$ ages of about 2500 Ma and 2335 Ma (Fig. 5A). They most probably represent ages of the paragneiss sedimentary protoliths. A selected population of discordant zircon grains yielded an upper intercept of a Discordia straight line at 2160 ± 8 Ma (Fig. 5A). The alignment along the same Discordia straight line towards a zero lower intercept indicates important and relatively recent Pb loss. The older zircon grains show igneous oscillatory zoning, but the younger ones demonstrate patchy and convolute zoning (Fig. 6), which are textures of local recrystallization at medium to high temperature metamorphism (Corfu *et al.* 2003).

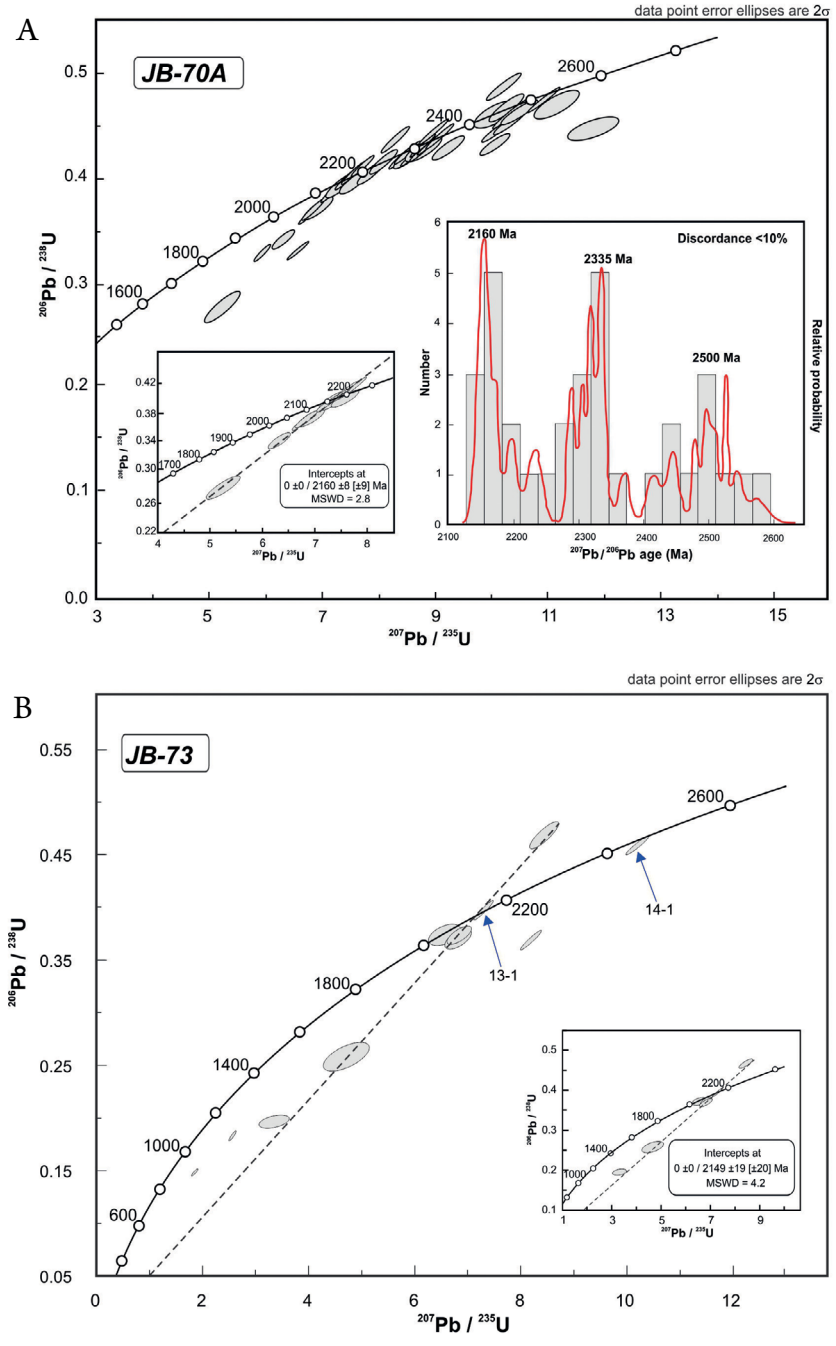

Figure 5. Concordia diagrams with the analytical points of zircon grains from Maribel area: (A) Sample JB-70A; (B) Sample JB-73.

Migmatitic orthogneiss JB-73

This granitic rock from Maribel is banded showing schlieren and granitic bands (Fig. 4D). Banding and schlieren could be syn-emplacement structures resulting from the stretching of magmatic enclaves or boudinage of mafic dikes by sub-magmatic flow. However, these structures are also seen in migmatites and are common in the leucosome of migmatites transitional between metatexite and diatexite (Sawyer 2008). The porphyroclast and granoblastic fabrics (Fig. 4E) could be formed by solid state flow, which are usual in migmatites (Sawyer 2008).

The granoblastic recrystallization of K-feldspar and plagioclase crystals (Fig. 4E) was probably formed by boundary-grain migration at high temperature (> 550ºC), as indicated by Passchier and Trouw (2005). However, mortar texture of quartz and K-feldspar (Fig. 4F) indicates mechanical crushing of the porphyroclastic and granoblastic fabrics, as well as recrystallization at lower temperatures (ca. 300ºC) through sub-grain rotation (Passchier and Trouw 2005).

Most zircon grains in this sample present high common Pb (Tab. 2), and seven are almost aligned (MSWD = 4.2) along a Discordia line with 2149 ± 20 Ma (Fig. 5B). Three of them yielded an upper intercept age of 2155 ± 8 Ma in the same Concordia diagram, which is interpreted as the possible age of leucosome formation of this migmatitic orthogneiss. The near-concordant zircon 13-1, bearing very little common Pb, supports this age. Another near-concordant zircon, 14-1 (Fig. 5B), with an age close to 2450 Ma, may be interpreted as an inherited grain. The $^{232}Th/^{238}U$ ratios of 0.14 to 0.80 (Tab. 2) are typical of igneous zircon grains (Hoskin and Schaltegger 2003). Patchy zoning is present in zircons of this granitic orthogneiss (Fig. 6), as well as fracturing and alteration pathways and metamict zones, indicating a late alteration (Corfu *et al.* 2003). The most altered zircon grains have high common-Pb (> 1.0 in Tab. 3).

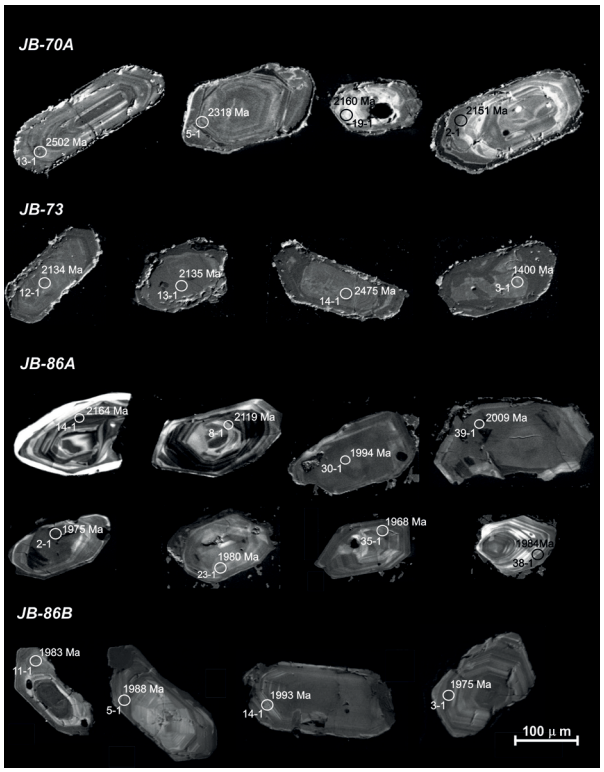

Figure 6. Cathodoluminescence (CL) images of some zircon crystals with their SHRIMP spots and respective $^{207}Pb/^{206}Pb$ ages. Some of them exhibit igneous oscillatory zoning, convolute and patchy zoning of local recrystallization, fracturing, metamictic zones and alteration pathways.

Migmatitic orthogneiss JB-86B

This migmatitic orthogneiss from Morro Grande is a banded granite with schlieren, stromatic, and net structures (Fig. 7A). The estimated degree of a partial melting structure (60%) corresponds to that of a transitional migmatite (Sawyer 2008). The melanosome (dark portion) is present, but the paleosome is not distinguished. Leucosome or neosome presents porphyroclasts of K-feldspar, quartz, and plagioclase in a granoblastic matrix of quartz-feldspar grains that show interlobate and polygonal grain boundaries (Figs. 7B and 7C), which indicate high-temperature recrystallization (Passchier and Trouw 2005).

Zircon grains generally show igneous oscillatory zoning, radial fracturing, and local patchy zoning (Fig. 6). In the Concordia diagram of Figure 8, the zircon grains are discordant and yielded a Discordia straight line with a combined weighted mean $^{207}Pb/^{206}Pb$ age of 1983 ± 5 Ma (MSWD = 1.2). It can be interpreted as the crystallization age of the leucosome, which is possibly related to the partial melting of the igneous protolith of this migmatitic rock. The calculated Concordia age of 1979 ± 8 Ma is another way to its calculation (Fig. 8A).

Muscovite gneiss JB-86A

This muscovite gneiss from Morro Grande presents migmatitic structures, as well as a discrete foliation, without banding (Fig. 7D). It shows rotated porphyroblasts of muscovite, porphyroclasts of quartz, and K-feldspar in a granolepidoblastic groundmass (Fig. 7E), with aggregates of fibro-radiated and elongated flakes of muscovite, as well as inter-lobated and polygonal granoblastic aggregates of quartz and K-feldspar (Fig. 7F). The presence of muscovite (30–40%) and absence of orthopyroxene indicate the rocks did not attain granulite-facies metamorphic conditions (Pattison *et al.* 2003, Bucher and Grapes 2011).

Most of the grains were near the Concordia in Figure 7B, and the weighted mean $^{207}Pb/^{206}Pb$ age of 1990 ± 3 Ma (MSWD = 1.3) for 22 points could be easily interpreted as a magmatic crystallization age. However, in the same diagram, many zircons were aligned along a Discordia straight line of 1981 ± 6 Ma, indicating Pb loss. The apparent $^{207}Pb/^{206}Pb$ ages between 2120 and 2180 Ma of four other zircon grains (Fig. 7B) are surely due to inherited material. Their ages are like those of granitic rocks from Maribel. Igneous oscillatory zoning is preserved in the zircon grains of 2119, 2164 and between 1968 and 1984 Ma, but it becomes blurred in the grains of 1994 and 2009 Ma (Fig. 6).

DISCUSSION AND CONCLUSIONS

The pelitic paragneiss JB-70A could represent the basis of a volcano-sedimentary sequence that underwent high-grade metamorphism. The oldest zircon grains furnished Neoarchean

Table 2. Summary of SHRIMP U–Pb zircon data for samples JB-70A and JB-73 from Maribel area.

spot	Pb_C	Pb*	U	Th	Th/U	$^{207}Pb/^{235}U$	err	$^{206}Pb/^{238}U$	err	$^{207}Pb/^{206}Pb$	err	Rho	$^{206}Pb/^{238}U^a$	1σ	$^{207}Pb/^{206}Pb^a$	1σ	Disc
	(%)	(ppm)	(ppm)	(ppm)			(%)		(%)		(%)		(Ma)		(Ma)		(%)
Pelitic paragneiss JB-70A																	
1-1	0.59	43	124	87	0.73	7.8441	1.2	0.4060	1.1	0.1401	0.5	0.896	2196	21	2229	9	2
2-1	0.47	129	389	128	0.34	7.1779	1.1	0.3884	1.0	0.1340	0.3	0.954	2115	18	2151	6	2
3-1	6.35	115	317	121	0.39	11.7885	1.5	0.4473	1.0	0.1911	1.1	0.663	2383	20	2752	19	16
4-1	1.76	99	264	175	0.68	10.0592	1.1	0.4453	1.0	0.1638	0.3	0.954	2375	21	2495	5	6
5-1	0.10	194	525	144	0.28	8.7780	1.0	0.4315	1.0	0.1475	0.2	0.979	2312	19	2318	4	0
6-1	0.48	88	222	107	0.50	10.3197	1.3	0.4614	1.2	0.1622	0.3	0.970	2446	25	2479	5	2
7-1	3.12	227	627	328	0.54	10.0555	1.1	0.4329	1.0	0.1685	0.5	0.889	2319	19	2542	8	10
8-1	0.71	139	382	241	0.65	8.7647	1.0	0.4270	1.0	0.1489	0.3	0.961	2292	19	2333	5	2
9-1	2.82	35	121	50	0.42	6.3078	1.3	0.3430	1.1	0.1334	0.8	0.819	1901	18	2143	13	13
10-1	2.64	176	637	206	0.33	5.9531	1.1	0.3301	1.0	0.1308	0.4	0.926	1839	16	2109	7	15
11-1	0.31	96	268	78	0.30	8.3863	1.1	0.4201	1.0	0.1448	0.3	0.961	2261	19	2285	5	1
12-1	0.14	260	713	118	0.17	8.5059	1.1	0.4245	1.0	0.1453	0.3	0.961	2281	20	2291	5	1
13-1	0.77	71	179	202	1.17	10.4920	1.2	0.4627	1.1	0.1645	0.6	0.868	2451	21	2502	10	2
14-1	-	85	225	166	0.76	9.0720	1.2	0.4406	1.1	0.1493	0.3	0.966	2353	22	2338	5	-1
15-1	0.06	119	301	68	0.23	10.0496	1.5	0.4606	1.1	0.1582	1.0	0.750	2442	23	2437	17	0
16-1	0.47	163	440	148	0.35	8.9138	1.2	0.4333	1.1	0.1492	0.3	0.970	2321	22	2337	5	1
17-1	0.02	92	258	128	0.51	8.0893	1.3	0.4162	1.1	0.1410	0.6	0.892	2243	21	2239	10	-0
18-1	-	66	173	137	0.82	8.2892	1.2	0.4372	1.2	0.1375	0.4	0.938	2338	23	2196	8	-8
19-1	0.42	36	105	73	0.72	7.3191	1.4	0.3941	1.2	0.1347	0.8	0.845	2142	22	2160	13	1
20-1	4.15	171	624	257	0.42	6.5623	1.1	0.3324	1.1	0.1432	0.3	0.970	1850	18	2266	5	21
21-1	-	152	395	235	0.61	8.9740	1.1	0.4443	1.1	0.1465	0.2	0.979	2370	22	2305	4	-3
22-1	0.07	100	249	128	0.53	10.2528	1.2	0.4674	1.1	0.1591	0.5	0.922	2472	23	2446	8	-1
23-1	0.86	193	534	153	0.30	8.6275	1.1	0.4230	1.1	0.1479	0.3	0.964	2274	21	2322	5	2
24-1	-	81	236	95	0.42	7.4555	1.2	0.4015	1.1	0.1347	0.4	0.954	2176	21	2160	6	-1
25-1	1.50	155	497	222	0.46	6.7840	1.2	0.3674	1.1	0.1339	0.4	0.939	2017	19	2150	7	7
26-1	1.54	114	286	213	0.77	11.1239	1.5	0.4704	1.1	0.1715	1.0	0.758	2485	23	2573	16	4
27-1	1.35	343	944	354	0.39	9.2275	1.3	0.4291	1.1	0.1560	0.6	0.884	2302	22	2412	10	5
28-1	0.05	176	501	277	0.57	7.5464	1.1	0.4065	1.1	0.1346	0.3	0.966	2199	20	2159	5	-2
29-1	1.18	125	396	223	0.58	6.8433	1.2	0.3717	1.1	0.1335	0.5	0.923	2037	19	2145	8	6
30-1	0.45	88	240	95	0.41	8.8004	1.5	0.4286	1.1	0.1489	0.9	0.896	2300	22	2333	16	2
Pelitic paragneiss JB-70A																	
31-1	-	92	214	96	0.46	10.2196	1.3	0.4870	1.2	0.1522	0.5	0.779	2558	24	2371	8	10
32-1	-	117	328	152	0.48	7.7119	1.1	0.4121	1.1	0.1357	0.3	0.922	2224	21	2174	4	-3
33-1	1.98	145	399	80	0.21	8.5951	1.5	0.4238	1.4	0.1471	0.7	0.975	2278	27	2312	12	2
34-1	0.37	190	469	394	0.87	10.9191	1.1	0.4745	1.1	0.1669	0.2	0.896	2503	23	2527	3	1
35-1	5.00	212	924	247	0.28	5.2430	2.3	0.2800	2.1	0.1358	1.1	0.987	1591	29	2174	20	30
36-1	1.47	160	415	291	0.72	10.3323	1.2	0.4533	1.1	0.1653	0.4	0.874	2410	22	2511	6	5
37-1	2.02	38	121	83	0.71	6.9279	1.5	0.3726	1.2	0.1349	0.8	0.945	2041	21	2162	14	7
38-1	0.84	134	396	170	0.44	7.5420	1.4	0.3971	1.1	0.1377	0.8	0.837	2156	20	2199	14	2
Migmatitic orthogneiss JB-73																	
1-1	0.87	294	1326	724	0.56	4.6731	3.8	0.2581	2.2	0.1313	3.1	0.591	1480	30	2116	54	34
2-1	1.30	94	296	91	0.32	6.8084	1.5	0.3697	1.0	0.1336	1.1	0.691	2028	18	2145	19	6
3-1	0.54	192	1500	97	0.07	1.8201	1.1	0.1487	0.9	0.0888	0.6	0.837	893	8	1400	12	39
4-1	0.11	202	1281	81	0.07	2.5217	1.0	0.1839	0.9	0.0995	0.4	0.930	1088	9	1614	7	35
5-1	0.37	59	184	67	0.38	6.5787	2.0	0.3720	1.1	0.1283	1.7	0.525	2039	19	2074	30	2
6-1	0.42	117	812	108	0.14	2.0195	9.5	0.1676	6.3	0.0874	7.0	0.671	999	59	1369	135	29
9-1	0.13	78	195	116	0.61	8.4496	1.3	0.4664	1.1	0.1314	0.8	0.814	2468	22	2117	13	20
10-1	2.17	196	1163	327	0.29	3.3210	3.5	0.1963	1.4	0.1227	3.2	0.388	1155	14	1996	57	46
11-1	0.02	204	646	389	0.62	8.1869	1.2	0.3681	1.2	0.1613	0.2	0.988	2020	21	2469	3	21
12-1	0.61	114	356	169	0.49	6.8444	1.4	0.3740	1.0	0.1327	0.9	0.744	2048	18	2134	16	5
13-1	-	141	416	254	0.63	7.3234	1.0	0.3950	1.0	0.1345	0.2	0.971	2146	18	2157	4	1
14-1	0.31	2157	471	366	0.80	10.2215	1.0	0.4581	1.0	0.1618	0.2	0.973	2431	20	2475	4	2

Errors are 1σ; Pb_c: total common ^{206}Pb; Pb*: radiogenic portion ^{206}Pb; Th/U: $^{232}Th/^{238}U$; Rho: correlation of errors; ^{a}: common Pb corrected using measured ^{204}Pb.

Table 3. Summary of SHRIMP U–Pb zircon data for samples JB-86A and JB-86B from Morro Grande area.

spot	Pb_c (%)	Pb* (ppm)	U (ppm)	Th (ppm)	Th/U	$^{207}Pb/^{235}U$	err (%)	$^{206}Pb/^{238}U$	err (%)	$^{207}Pb/^{206}Pb$	err (%)	Rho	$^{206}Pb/^{238}U^a$ (Ma)	1σ	$^{207}Pb/^{206}Pb^a$ (Ma)	1σ	Disc. (%)
Muscovite gneiss JB-86A																	
2-1	0.29	59	196	145	0.77	5.7385	1.8	0.3501	1.7	0.1189	0.5	0.955	1935	28	1939	9	0
2-2	0.97	127	422	690	1.69	5.8710	1.6	0.3511	1.5	0.1213	0.5	0.949	1940	26	1975	9	2
3-1	0.99	161	530	443	0.86	5.9772	1.6	0.3553	1.5	0.1220	0.5	0.942	1960	26	1986	10	1
4-1	2.13	82	270	278	1.06	6.7777	1.7	0.3615	1.5	0.1360	0.6	0.924	1989	26	2177	11	10
5-1	3.03	87	336	602	1.85	5.1991	1.9	0.3073	1.8	0.1227	0.6	0.952	1727	28	1996	10	15
6-1	0.49	47	156	163	1.08	5.9535	1.7	0.3542	1.6	0.1219	0.5	0.951	1954	27	1984	9	2
7-1	4.37	39	185	137	0.77	4.3773	1.8	0.2566	1.7	0.1237	0.7	0.927	1472	22	2011	12	30
8-1	1.36	57	183	80	0.45	6.6254	1.6	0.3652	1.6	0.1316	0.5	0.960	2007	27	2119	8	6
9-1	0.92	126	423	568	1.39	5.9222	1.5	0.3494	1.5	0.1229	0.3	0.981	1932	25	1999	5	4
10-1	2.15	23	87	126	1.50	5.3392	1.9	0.3180	1.6	0.1218	0.9	0.881	1780	25	1982	16	12
11-1	0.93	66	225	262	1.20	5.7764	1.6	0.3431	1.5	0.1221	0.4	0.970	1901	25	1987	7	5
12-1	-	125	400	608	1.57	6.0930	1.5	0.3639	1.5	0.1214	0.3	0.986	2001	26	1978	5	-1
13-1	-	38	119	109	0.95	6.1621	1.7	0.3699	1.6	0.1208	0.6	0.945	2029	28	1968	10	-4
14-1	0.13	39	112	65	0.60	7.5299	1.7	0.4045	1.6	0.1350	0.6	0.938	2190	30	2164	10	-1
15-1	0.28	104	340	310	0.94	5.9863	1.6	0.3562	1.5	0.1219	0.3	0.979	1964	26	1984	6	1
16-1	1.49	58	214	177	0.86	5.2904	1.6	0.3214	1.6	0.1194	0.5	0.950	1797	24	1947	9	9
17-1	0.31	118	386	530	1.42	5.9724	1.5	0.3558	1.5	0.1217	0.3	0.982	1962	26	1982	5	1
18-1	-	112	370	145	0.41	5.6062	1.8	0.3505	1.7	0.1160	0.4	0.974	1937	29	1896	7	-3
19-1	1.96	76	279	212	0.78	5.4448	1.6	0.3218	1.5	0.1227	0.6	0.933	1799	24	1996	10	11
20-1	0.38	161	531	718	1.40	5.9492	1.5	0.3532	1.5	0.1222	0.2	0.990	1950	25	1988	4	2
21-1	0.29	55	177	237	1.38	6.0334	1.6	0.3582	1.6	0.1222	0.4	0.967	1974	26	1988	7	1
22-1	0.41	226	763	389	0.53	5.6928	1.5	0.3453	1.5	0.1196	0.2	0.990	1912	25	1950	4	2
23-1	0.33	47	155	141	0.94	5.9356	1.6	0.3541	1.6	0.1216	0.4	0.969	1954	26	1980	7	1
24-1	0.03	212	682	542	0.82	6.0370	1.5	0.3611	1.5	0.1212	0.3	0.980	1987	26	1975	5	-1
25-1	-	98	309	246	0.82	6.1067	1.6	0.3681	1.5	0.1203	0.4	0.967	2020	27	1961	7	-4
26-1	2.71	33	113	121	1.11	5.7132	5.1	0.3431	1.8	0.1208	4.8	0.352	1902	30	1968	86	4
27-1	0.65	41	150	143	0.99	4.8656	2.0	0.3185	1.7	0.1108	1.1	0.848	1782	26	1812	19	2
28-1	2.31	37	131	79	0.62	6.2041	1.6	0.3404	1.6	0.1322	0.5	0.961	1888	26	2127	8	13
29-1	1.52	56	201	171	0.88	5.5210	2.3	0.3288	1.9	0.1218	1.1	0.862	1833	31	1982	20	9
30-1	0.10	168	543	395	0.75	6.0998	1.8	0.3609	1.8	0.1226	0.2	0.994	1986	31	1994	3	0
31-1	2.15	71	268	277	1.07	5.2904	1.9	0.3136	1.9	0.1223	0.4	0.978	1759	29	1991	7	13
32-1		92	339	178	0.54	5.2537	1.9	0.3192	1.8	0.1194	0.7	0.938	1786	28	1947	12	9
33-1	1.13	66	228	242	1.10	5.7394	1.6	0.3390	1.5	0.1228	0.4	0.974	1882	25	1997	6	7
34-1	0.98	44	145	172	1.22	6.1067	3.4	0.3533	1.6	0.1254	3.1	0.456	1950	26	2034	54	5
35-1	0.35	74	244	165	0.70	5.8676	1.6	0.3522	1.5	0.1208	0.4	0.974	1945	26	1968	6	1
36-1	0.97	126	433	438	1.04	5.7658	1.5	0.3416	1.5	0.1224	0.3	0.987	1894	25	1992	4	6
37-1	0.70	51	170	227	1.37	5.9063	1.6	0.3498	1.6	0.1224	0.4	0.965	1934	26	1992	8	3
38-1	1.04	51	172	235	1.41	5.7915	1.6	0.3446	1.6	0.1219	0.5	0.949	1909	26	1984	9	4
39-1	0.38	81	264	249	0.97	6.1327	1.7	0.3599	1.5	0.1236	0.6	0.931	1982	26	2009	11	2
Migmatitic orthogneiss JB-86B																	
1-1	0.02	38	132	167	1.31	5.6975	1.1	0.3391	1.0	0.1218	0.4	0.919	1883	16	1983	7	6
2-1	0.18	84	289	269	0.96	5.6614	1.0	0.3364	0.9	0.1220	0.4	0.932	1869	15	1986	6	7
3-1	0.09	51	172	123	0.74	5.8133	1.0	0.3477	0.9	0.1213	0.4	0.921	1924	16	1975	7	3
4-1	0.89	60	201	145	0.75	5.7774	1.6	0.3478	0.9	0.1205	1.2	0.600	1924	16	1963	22	2
5-1	0.33	31	99	58	0.60	6.0148	1.4	0.3572	1.3	0.1221	0.7	0.890	1969	22	1988	12	1
6-1	0.81	62	227	230	1.05	5.2730	1.1	0.3163	0.9	0.1209	0.6	0.850	1771	14	1970	10	12
7-1	0.07	44	147	84	0.59	5.8783	1.0	0.3505	0.9	0.1216	0.4	0.916	1937	16	1980	7	3
8-1	0.17	59	197	121	0.63	5.8901	1.0	0.3482	0.9	0.1227	0.4	0.908	1926	15	1996	8	4
9-1	0.68	69	275	118	0.44	4.8662	1.1	0.2929	0.9	0.1205	0.6	0.854	1656	13	1963	10	18
10-1	0.39	57	197	182	0.95	5.6841	1.3	0.3366	1.2	0.1225	0.5	0.928	1870	19	1993	9	7
11-1	0.13	63	205	158	0.80	5.9637	1.0	0.3550	0.9	0.1218	0.4	0.926	1958	16	1983	7	1
12-1	0.21	93	312	202	0.67	5.8247	1.0	0.3459	0.9	0.1221	0.4	0.930	1915	15	1987	6	4
13-1	0.15	57	191	149	0.81	5.7773	1.0	0.3458	0.9	0.1212	0.4	0.918	1914	15	1974	7	3
14-1	0.19	54	174	151	0.90	6.0734	1.2	0.3596	1.1	0.1225	0.5	0.914	1980	19	1993	9	1

Errors are 1σ; Pb_c: total common ^{206}Pb; Pb*: radiogenic portion ^{206}Pb; Th/U: $^{232}Th/^{238}U$; Rho: correlation of errors; ^{a}: common Pb corrected using measured ^{204}Pb.

ages around 2500–2540 Ma, but this rock also includes many younger detrital sources within the 2500–2160 Ma time interval. The histogram inserted in Figure 4A shows three clear peaks at about 2500, 2335 and 2160 Ma, associated with the magmatic crystallization of different groupings of detrital zircons, which may represent the timing of successive magmatic pulses in the regional tectonic history. In addition, as the rock did not present migmatitic structures and was not cut by granitic veins, its Rhyacian zircon grains could represent a younger detrital source and, hence, a maximum age for sediment deposition.

The migmatitic orthogneiss JB-73 presents mesoscopic migmatitic structures, but its microstructures and

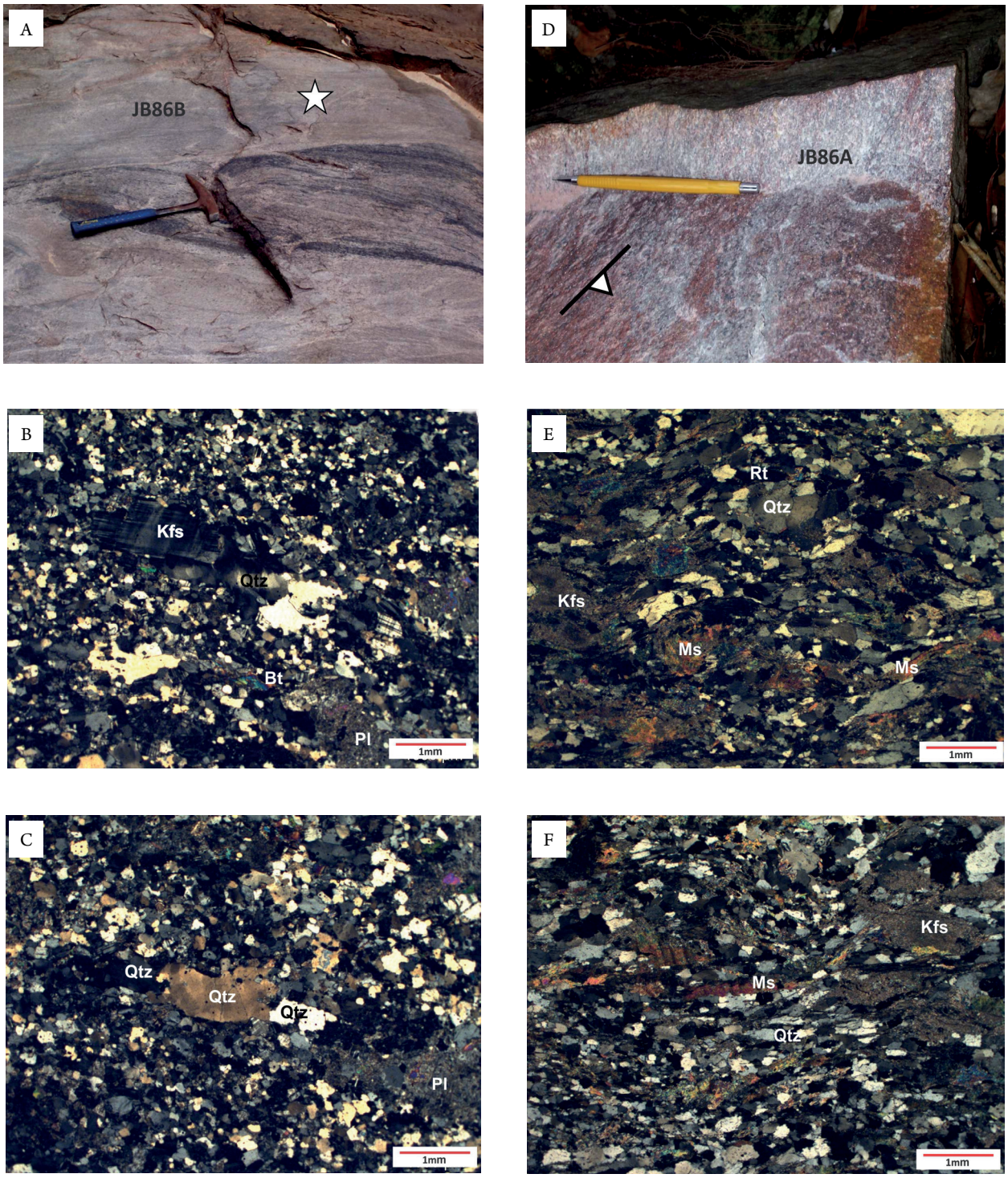

Figure 7. Basement rocks of Morro Grande area. All microphotographs of thin sections were taken in crossed polarized light. JB-86B migmatitic orthogneiss sample: (A) Granitoid bands, schlieren, stromatic and net structures (star — selected part); (B) Porphyroclasts of K-feldspar (Kfs), quartz (Qtz) and altered (sericite) plagioclase (Pl) in a granoblastic matrix of quartz and feldspar grains with interlobate and polygonal grain boundaries and recrystallized flakes; biotite (Bt); (C) Ribbons of porphyroclasts of quartz (Qtz) and rounded porphyroclasts of altered (sericite) plagioclase (Pl); (D) Discrete foliation of the muscovite gneiss JB-86A muscovite gneiss sample: (E) Rotated porphyroblast of muscovite (Ms), relict grains of quartz (Qtz) and K-feldspar (Kfs) in a granolepidoblastic matrix with rutile (Rt) crystals; (F) Porphyroclast of altered plagioclase (Pl), aggregates of muscovite flakes (Ms) and elongated grains of quartz (Qtz) in an interlobate and polygonal granoblastic matrix.

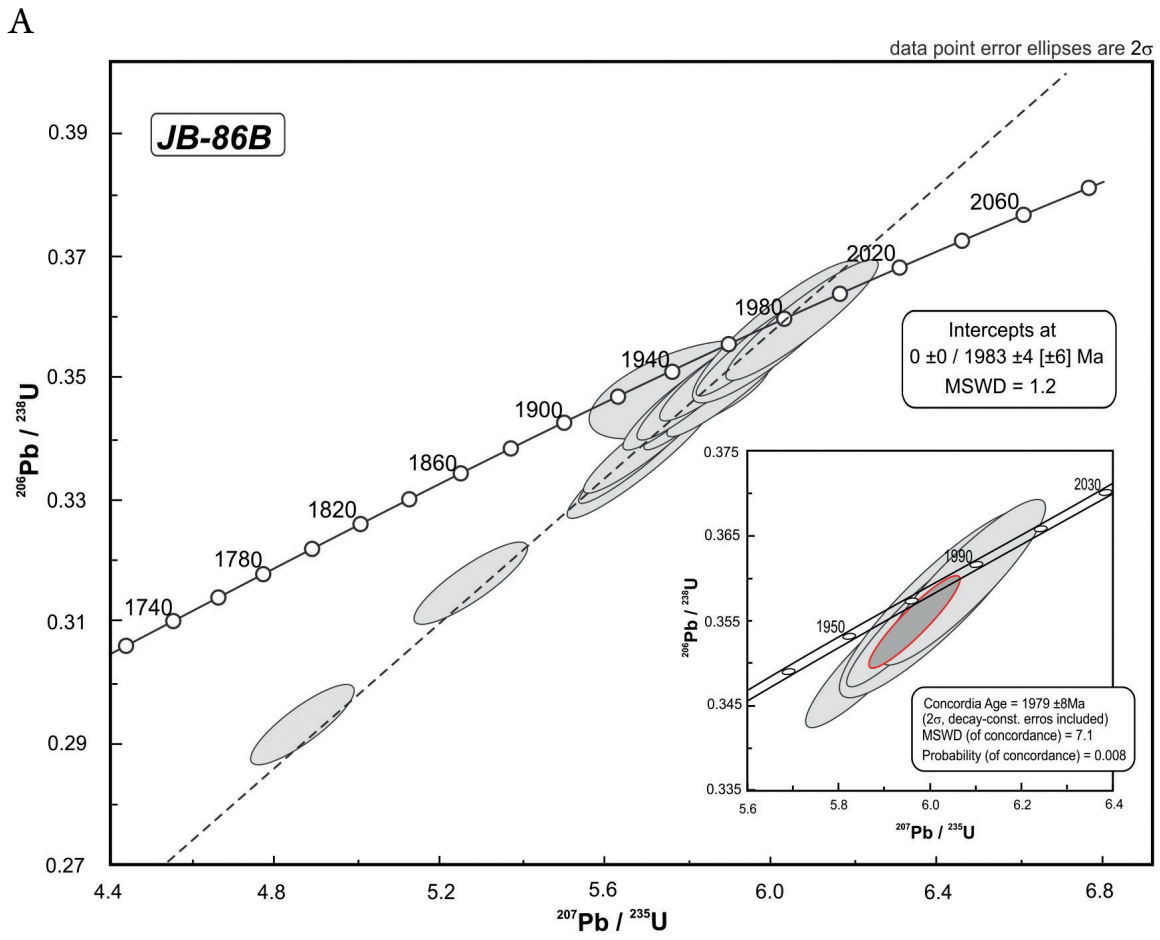

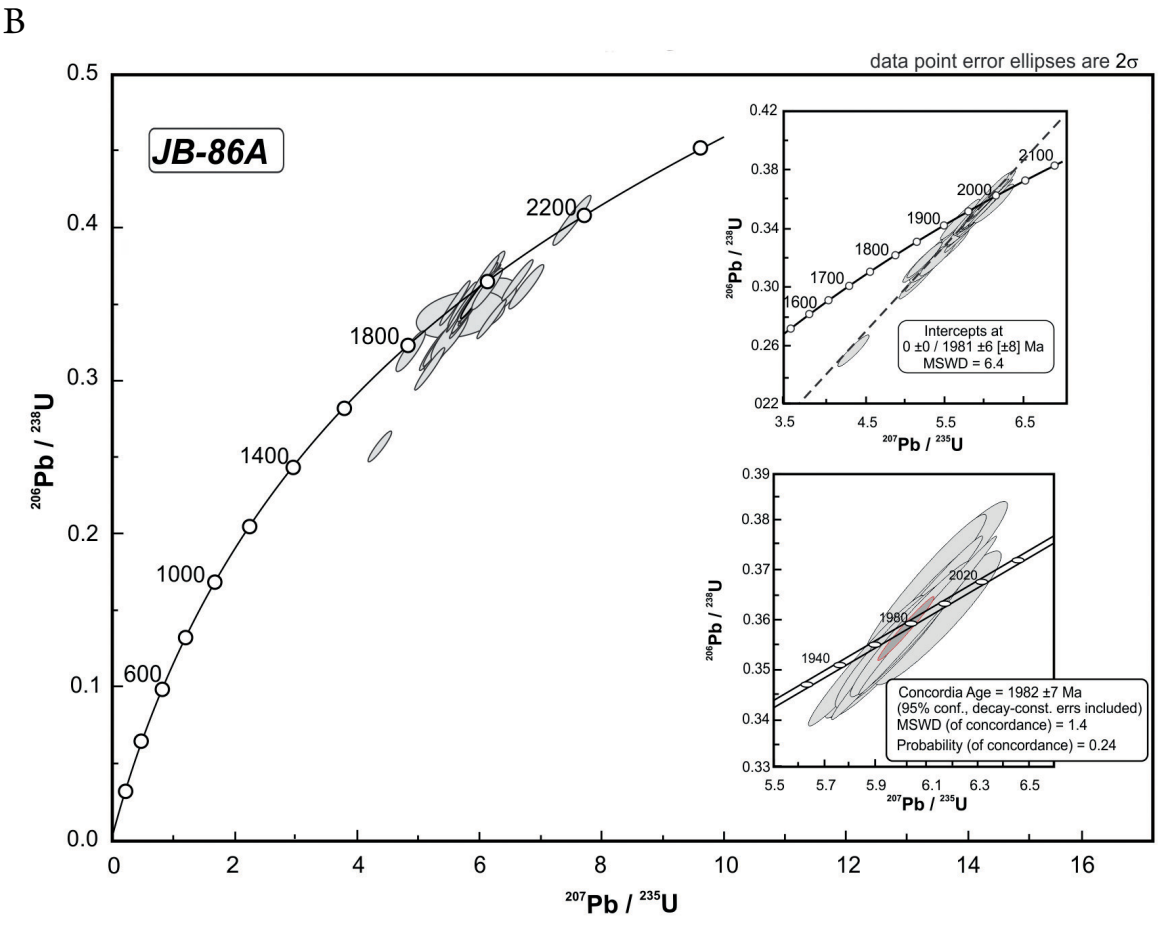

Figure 8. Concordia diagrams with analytical points of zircon grains from Morro Grande area: (A) Sample JB-86B; (B) Sample JB-86A.

micro-textures give no conclusive evidence that it was formed through anatexis. The single concordant zircon grain of 2470 Ma shown in Figure 5B may be a xenocryst of the wall rocks or an inherited crystal from partial melting of the protolith. This rock was dated by means of 12 zircon grains in the Concordia diagram of Figure 5B, in which most analytical points were aligned along a Discordia straight line, where the three best aligned grains yielded 2155 ± 8 Ma, interpreted as the possible crystallization age of the leucosome. A magmatic event of similar age (2160 ± 8 Ma) was obtained from the youngest detrital population of the paragneiss JB-70A, located in the same region and, therefore, subjected to the same tectonic evolution. The 2160–2150 Ma magmatic/metamorphic ages yielded by JB-70 and JB-73 are coeval with the Rhyacian tectono-metamorphic episode characteristic of the nearby Bacajá tectonic domain, which occurs to the east of the IXD.

Indeed, pelitic and pelite-psamitic paragneisses with Mesoarchean to Siderian detrital sources that underwent Rhyacian granulite metamorphism are widespread within the western Bacajá domain (Vasquez 2006, Vasquez *et al.* 2014). In addition, the Bacajá domain also contains granitoids of 2215–2154 Ma related to Rhyacian magmatic arcs (Vasquez *et al.* 2008a, Macambira *et al.* 2009), as well as older igneous rocks yielding ages from ca. 2670 to 2300 Ma (Vasquez *et al.* 2008a, Macambira *et al.* 2009). Rocks with such ages could have produced detrital zircons for the protolith of the JB-70A paragneiss. Therefore, considering the possible Rhyacian age of sample JB-73 (Fig. 5B), and the Neoarchean to Rhyacian detrital zircons of sample JB-70A (Fig. 5A), we may propose a correlation of the Maribel basement rocks with the Bacajá domain. This is supported by the relatively close occurrence (< 10 km) of the basement windows to the Bacajá domain (Fig. 2).

The medium to high-grade rocks, JB-86A and JB-86B, are located very close together and they therefore must have undergone the same conditions of metamorphism and ductile deformation. Their Concordia ages (Figs. 8A and 8B) are identical within experimental error, confirming the robust significance of the ca. 1980–1990 Ma age, which is the crystallization age of the igneous protolith.

The muscovite gneiss JB-86A does not have banding and mineral assemblages of granulite facies metamorphism, but its polygonal micro-texture (Fig. 7F) indicates granoblastic recrystallization at high-temperature (>550ºC), corresponding to amphibolite facies metamorphism. Due to the 1982 ± 7 Ma Concordia age of this sample (Fig. 8B), we tentatively consider this as the magmatic crystallization age of a volcanic rock that underwent a potassic hydrothermal alteration before the amphibolite facies metamorphism.

The migmatitic orthogneiss JB-86B presents some typical migmatitic structures that correspond to a transitional migmatite, as characterized by Sawyer (2008). Its porphyroclastic and granoblastic micro-textures are typical of a high-temperature solid state deformation. The dated sample very probably corresponds to a portion of the leucosome of this migmatite, which does not include inherited zircon grains. The Concordia diagram of Figure 8A shows the age of 1979 ± 8 Ma, identical, within analytical error, with that of sample JB-86A. This age could represent the anatexis time that formed this migmatite. If this is so, Morro Grande area is the first piece of evidence of formation of igneous rocks of ca. 1980 by partial melting of old crust in the southern part of the Amazonian craton.

The granitoid emplacement climax within the large NW-SE transcurrent shear zones of Tapajós domain occurred between 2000 and 1960 Ma (Vasquez *et al.* 2002, 2008b). The same magmatic event is also present in the IXD (Padilha and Barros 2008, Alves *et al.* 2010, Semblano *et al.* 2016), and many of its rocks exhibit preserved igneous textures with local protomylonitic textures. High-temperature recrystallization and migmatitic structures identified in these rocks of Morro Grande are the first occurrence of high-grade metamorphic rocks formed at about 1980 Ma in the area of the IXD. It is also the first piece of evidence of an Orosirian high-grade metamorphism in the Central Brazil shield, which forms the southern half of the Amazonian craton.

Tassinari *et al.* (2004) identified a high-grade metamorphism of ca. 1.98 Ga in the northwestern corner of the Guiana shield, which is associated with the exhumation that followed high-grade metamorphism of Imataca Complex at 2.07–2.05 Ga. This situation of two successive episodes of high-grade metamorphism is similar to that encountered in the Bakhuis granulite belt of the central part of the shield, in which a late episode of 1.99 to 1.95 Ga succeeded the main high-grade regional metamorphism of the area (2.07 to 2.05 Ga). It has been considered as a late high-grade metamorphism of the Trans-Amazonian cycle (De Roever *et al.* 2015, Klaver *et al.* 2015, Kroonenberg *et al.* 2016). Moreover, the ca. 1.98 Ga Orocaima igneous belt formed essentially by felsic volcanic rocks and granites (Reis *et al.* 2000) is widespread through the entire Guiana shield, comprising from Venezuela in the west to Suriname in the east, the Cuchivero, Surumu, Iwokrama and Dalbana units.

ACKNOWLEDGEMENTS

We thank the financial support received for the analytical work with the SHRIMP equipment at Universidade de São Paulo (USP), which was provided by grant 2013/12754-0 of the Research Foundation of the State of São Paulo (FAPESP, acronym in Portuguese). We would also like to thank the careful review performed by Robert J. Pankhurst and by an anonymous reviewer for the Brazilian Journal of Geology.

ARTICLE INFORMATION
Manuscript ID: 20190067. Received on: 07/27/2019. Approved on: 09/27/2019.
MV wrote the manuscript, prepared figures and tables, discussed geochronology and petrography data, corrected the manuscript, mapped the geology, selected samples, managed geological mapping funding. UC wrote and improved the manuscript, discussed geochronology data, managed financial support of geochronology. KS acquired and treated geochronological data. JB mapped the geology, collected samples, discussed petrology. TF carried out petrography analysis, discussed petrology and VM prepared samples and acquired geochronological data.
Competing interests: The authors declare no competing interests.

REFERENCES

Alves C.L., Sabóia A.M., Martins E.G., Stropper J.L. 2010. *Folhas São José do Xingu e Comandante Fontoura, Escala 1:250.000*. Projeto Noroeste-Nordeste de Mato Grosso. Goiânia: Companhia de Pesquisas de Recursos Minerais – CPRM. 120 p. Available at: <http://rigeo.cprm.gov.br/jspui/handle/doc/11197>. Accessed on: Sept 30, 2019.

Barreto C.J.S., Lafon J.M., Rosa-Costa L.T., Lima E.F. 2014. Paleoproterozoic (~1.89 Ga) felsic volcanism of the Iricoumé Group, Guyana Shield, South America: geochemical and Sm-Nd isotopic constraints on sources and tectonic environment. *International Geology Review*, **56**(11):1332-1356. https://doi.org/10.1080/00206814.2014.930800

Barros M.A.S., Padilha R.A., Rubert R.R., Pimentel M.M., Chemale JR.F. 2006. Iriri volcanism and Rio Dourado Granite: A-Type Paleoproterozoic Magmatism in northeastern Mato Grosso - Brazil. *In*: Symposium on magmatism, crustal evolution, and metallogenesis of the Amazonian Craton and Workshop on A-type granites and related rocks through time (IGCP 510). *Abstracts*... p. 39.

Barros M.A.S., Pimentel M.M., Rocha M.L.B.P., Silva F.R., Padilha R.A., Dantas E.L., Moura E. 2011. A Suíte Intrusiva Rio Dourado – um granito tipo A de 1,88 Ga - Sudeste do Craton Amazônico - Mato Grosso - Brasil. *Revista Geologia USP*, **11**(1):75-93. https://doi.org/10.5327/Z1519-874X2011000100005

Black L.P., Kamo S.L., Allen C.M., Davis D.W., Aleinikoff J. N., Valley J.W., Mundil R., Campbell I.H., Korsch R.J., Williams I.S., Foudoulis C. 2004. Improved $^{206}Pb/^{238}U$ microprobe geochronology by the monitoring of trace element related matrix effect; SHRIMP, ID-TIMS, ELA-ICP-MS and oxygen isotope documentation for a series of zircon standards. *Chemical Geology*, **205**(1-2):115-140. https://doi.org/10.1016/j.chemgeo.2004.01.003

Bucher K., Grapes R. 2011. Petogenesis of metamorphic rocks. Berlin: Springer. 428p.

Cordani U.G., Tassinari C.C.G., Kawashita K. 1984. A Serra dos Carajás como região limítrofe entre províncias tectônicas. *Ciências da Terra*, (9):6-11.

Cordani U.G., Tassinari C.C.G., Teixeira W., Basei M.A.S., Kawashita K. 1979. Evolução tectônica da Amazônia com base nos dados geocronológicos. *In*: Congreso Geologico Chileno, 2., Arica, Chile. *Actas*..., v. 4, p. 137-148.

Cordani U.G., Teixeira W. 2007. Proterozoic accretionary belts in the Amazonian Craton. *Geological Society of America Memoirs*, **200**:297-320. https://doi.org/10.1130/2007.1200(14)

Corfu F., Hanchar J.M., Hoskin P.W.O., Kinny P. 2003. Atlas of zircon textures. *Reviews in Mineralogy and Geochemistry*, **53**(1):469-500. https://doi.org/10.2113/0530469

Dall'Agnol R., Lafon J.M., Macambira M.J.B. 1994. Proterozoic anorogenic magmatism in the Central Amazonian Craton: geochronological and geochemical aspects. *Mineralogy and Petrology*, **50**(1-3):113-38. https://doi.org/10.1007/BF01160143

De Roever E.W.F., Lafon J.M., Delor C., Guerrot C. 2015. Orosirian magmatism and metamorphism in Suriname: new geological constraints. *In*: Gorayeb P.S.S., Lima A.M.M. (Eds.), *Contribuições à geologia da Amazônia*. Belém: Sociedade Brasileira de Geologia, 9, p. 343-356.

Fernandes C.M.D., Juliani C., Monteiro L.V.S., Lagler B., Echeverri Misas C.M. 2011. High-K calc-alkaline to A-type fissure-controlled volcano-plutonism of the São Félix do Xingu region, Amazonian craton, Brazil: Exclusively crustal sources or only mixed Nd model ages? *Journal of South American Earth Sciences*, **32**(4):351-368. https://doi.org/10.1016/j.jsames.2011.03.004

Hoskin P.W.O., Schaltegger U. 2003. The composition of zircon and igneous and metamorphic petrogenesis. *Reviews in Mineralogy and Geochemistry*, **53**(1):27-62. https://doi.org/10.2113/0530027

Juliani C., Fernandes C.M.D. 2010. Well-preserved Late Paleoproterozoic volcanic centers in São Felix do Xingu region, Amazonian Craton, Brazil. *Journal Volcanology and Geothermal Research*, **191**(3-4):167-179. https://doi.org/10.1016/j.jvolgeores.2010.01.016

Klaver M., De Roever E.W.F., Nane J.A.M., Mason P.R.D., Davies G.R. 2015. Charnockites and UHT metamorphism in the Bakhuis Granulite Belt, Western Suriname: Evidence for two separate UHT events. Precambrian Research, 262:1-19. http://dx.doi.org/10.1016/j.precamres.2015.02.014

Klein E.L., Rodrigues J.B., Queiroz J.D.S., Oliveira R.G., Guimarães S.B., Chaves C.L. 2016. Deposition and tectonic setting of the Palaeoproterozoic Castelo de Sonhos metasedimentary formation, Tapajós Gold Province, Amazonian Craton, Brazil: age and isotopic constraints. *International Geology Review*, **59**(7):864-883. https://doi.org/10.1080/00206814.2016.1237311

Kroonenberg S.B., de Roever E.W.F., Fraga L.M., Reis N.J., Faraco M.T.J., Lafon J.M., Cordani U.G., Wong T.E. 2016. Paleoproterozoic evolution of the Guiana Shield in Surinam: a revised model. *Netherlands Journal of Geosciences*, **95**(4):491-522. https://doi.org/10.1017/njg.2016.10

Leal R.E., Lafon J.M., Rosa-Costa L.T., Dantas E.L. 2018. Orosirian magmatic episodes in the Erepecuru-Trombetas domain (southeastern Guyana shield): Implications for the crustal evolution of the Amazonian craton. *Journal of South American Earth Sciences*, **85**:278-297. https://doi.org/10.1016/j.jsames.2018.04.011

Ludwig K.R. 2009a. *SQUID 2:* A User's Manual, rev. 12. Special Publication 5. Berkeley: Geochronology Center, 110 p.

Ludwig K.R. 2009b. *User's Manual for Isoplot 3.70*. Special Publication 4. Berkeley: Berkeley Geochronology Center, 76 p.

Macambira E.M.B., Vale A.G. 1997. *São Félix do Xingu:* Folha SB.22-Y-B, Estado do Pará, escala 1:250.000. Texto Explicativo, Programa Levantamentos Geológicos Básicos do Brasil. Brasília, Companhia de Pesquisas de Recursos Minerais – CPRM, 344 p. Available at: <http://rigeo.cprm.gov.br/jspui/handle/doc/8718>. Accessed on: Sept, 2019.

Macambira M.J.B., Vasquez M.L., Silva D.C.C., Galarza M.A., Barros C.E.M., Camelo J.F. 2009. Crustal growth of the central-eastern Paleoproterozoic domain, SE Amazonian craton: Juvenile accrecion vs. reworking. *Journal of South America Earth Sciences*, **27**(4):235-246. https://doi.org/10.1016/j.jsames.2009.02.001

Padilha R.A. 2007. *Petrologia e geoquímica dos granitos da Suíte Intrusiva Vila Rica e do Granito Rio Dourado – borda sudeste do Cráton Amazônico (Província Amazônia Central – Área Xingú-Iricoumé - nordeste de Mato Grosso)*. MSc Dissertation, Universidade Federal do Mato Grosso, Cuiabá, 120 p.

Padilha R.A., Barros M.A.S. 2008. Petrologia e geoquímica das suítes intrusivas Vila Rica e Rio Dourado - Província Amazônia Central, borda sudeste do Cráton Amazônico (MT). *Revista Brasileira de Geociências*, **38**(4):642-653. https://doi.org/10.25249/0375-7536.2008384642653

Passchier C.W., Trouw R.A.J. 2005. Microtectonics. 2ª ed. Berlin: Springer, 366 p.

Pattison D.R.M., Chacko T., Farquhar J., McFarlane C.R.M. 2003. Temperatures of granulite-facies metamorphism: constraints from experimental phase equilibria and thermobarometry corrected from retrograde exchange. *Journal of Petrology*, **44**(5):867-900. https://doi.org/10.1093/petrology/44.5.867

Pinho S.C.C., Fernandes C.M.D., Teixeira N.P., Paiva Junior A.L., Cruz V.L., Lamarão C.N., Moura C.A.V. 2006. O magmatismo paleoproterozóico da região de São Félix do Xingu, Província Estanífera do Sul do Pará: Petrografia e geocronologia. *Revista Brasileira de Geociências*, **36**(4):724-732. https://doi.org/10.25249/0375-7536.2006364724732

Reis N.J., Faria M.S.G, Fraga L.M., Haddad R.C. 2000. Orosirian calcalkaline volcanism and the Orocaima event in the Northern Amazonian Craton, Eastern Roraima State, Brazil. *Revista Brasileira de Geociências*, **30**(3):380-383. https://doi.org/10.25249/0375-7536.2000303380383

Sato K., Tassinari C.C.G. 1997. Principais eventos de acresção continental no Cráton Amazônico, baseados em idade modelo Sm-Nd, calculadas em evoluções de estágio único e estágio duplo. *In*: Costa M.L., Angélica R.S. (Eds.), *Contribuições à Geologia da Amazônia*. Belém: Sociedade Brasileira de Geologia, 1, p. 91-142.

Sato K., Tassinari C.C.G., Basei M.A.S., Siga Jr., O., Onoe A.T., Souza M.D. 2014. Sensitive High Resolution Ion Microprobe (SHRIMP IIe/MC) of the Institute of Geosciences of the University of São Paulo, Brazil: analytical method and first results. *Geologia USP, Série Científica*, **14**(3):3-18. https://doi.org/10.5327/Z1519-874X201400030001

Sawyer E.W. 2008. Working with migmatites: nomenclature for the constituent parts. *In*: Sawyer E.W. (Ed.). *Working with migmatites*. Canada: Mineralogical Association of Canada Short Course Series, 8, p. 1-28.

Semblano F.R.D., Pereira N.C.S., Vasquez M.L., Macambira M.J.B. 2016. Novos dados geológicos e isotópicos para o Domínio Iriri-Xingu, Província Amazônia Central; implicações para a idade do Grupo Iriri. *Revista do Instituto de Geociências - USP, Série Científica*, **16**(3):19-38. https://doi.org/10.11606/issn.2316-9095.v16i3p19-38

Silva G.G., Lima M.I.C., Andrade A.R.F., Issler R.S., Guimarães G. 1974. *Geologia Folhas SB.22 - Araguaia e parte da Folha SC.22 - Tocantins*. Projeto Radambrasil, Levantamento de Recursos Naturais. Rio de Janeiro: Departamento Nacional de Produção de Mineral – DNPM, 4, p. 1-143.

Stern R.A., Amelin Y. 2003. Assessment of errors in SIMS zircon U-Pb geochronology using natural zircon standard and NIST SRM 610 glass. *Chemical Geology*, **197**(1-4):111-142. https://doi.org/10.1016/S0009-2541(02)00320-0

Superintendência de Desenvolvimento da Amazônia (SUDAM), Geologia e Mineração Trabalhos Técnicos Ltda. (Geomitec). 1972. *Pesquisa Mineral no Iriri/Curuá*. Belém: SUDAM/Departamento de Recursos Naturais, 62 p.

Tassinari C.C.G., Macambira M.J.B. 1999. Geochronological provinces of the Amazonian Craton. *Episodes*, **22**(3):174-182.

Tassinari C.C.G., Macambira, M.J.B. 2004. A evolução tectônica do Cráton Amazônico. *In*: Mantesso-Neto V., Bartorelli A., Carneiro C.D.R., Brito Neves B.B. (Eds.). *Geologia do continente Sul-americano:* evolução da obra de Fernando Flávio Marques de Almeida. São Paulo: Beca, p. 471-485.

Tassinari C.C.G., Munhá J.M.V., Teixeira W., Palácios T., Nutman A.P., Sosa C.S., Santos A.P., Calado B.O. 2004. The Imataca Complex, NW Amazonian Craton, Venezuela: crustal evolution and integration of geochronological and petrological cooling histories. *Episodes*, **27**(1):3-12. https://doi.org/10.18814/epiiugs/2004/v27i1/002

Teixeira N.P., Fernandes C.M.D., Moura C.A.V., Pinho S.C.C., Bettencourt J.S. 2002. Geologia, geoquímica, geocronologia e isótopos de Sm-Nd de rochas vulcânicas paleoproterozóicas do Grupo Uatumã ocorrentes na região de São Félix do Xingu, Província Mineral de Carajás, Cráton Amazônico, Brasil. *In*: Simpósio sobre Vulcanismo e Ambientes Associados, 2. *Abstracts*... Belém, p. 28.

Vasquez M.L. 2006. *Geocronologia em zircão, monazita e granada e isótopos de Nd das associações litológicas da porção oeste do Domínio Bacajá: evolução crustal da porção meridional da província Maroni-Itacaiúnas, sudeste do Cráton Amazônico*. PhD Thesis, Universidade Federal do Pará, Belém, 212 p. Available at: <http://rigeo.cprm.gov.br/xmlui/bitstream/handle/doc/165/tese_marcelo_vasquez.pdf?sequence=1&isAllowed=y>. Accessed on: Sept, 2019.

Vasquez M.L., Macambira M.J.B., Armstrong R. 2008a. Zircon geochronology of granitoids from the western Bacajá domain, southeastern Amazonian craton, Brazil: Neoarchean to Orosirian evolution. *Precambrian Research*, **161**(3-4):279-302. https://doi.org/10.1016/j.precamres.2007.09.001

Vasquez M.L., Macambira M.J.B., Armstrong R.A. 2014. High grade metamorphism constrained by U-Pb SHRIMP ages: an example of the Bacajá Domain, Amazonian Craton, Brazil. *In*: South-American Symposium on Isotope Geology, 9. *Abstracts*… São Paulo, Brazil.

Vasquez M.L., Ricci P.S.F., Klein E.L. 2002. Granitóides pós-colisionais da porção leste da Província Tapajós. *In*: Klein E.L., Vasquez M.L., Rosa-Costa L.T. (Eds.), *Contribuições à Geologia da Amazônia*. Belém: Sociedade Brasileira de Geologia, 3, p. 67-84.

Vasquez M.L., Rosa-Costa L.T., Silva C.M.G., Klein E.L. 2008b. Compartimentação tectônica. *In*: Vasquez M.L., Rosa-Costa L.T. (Eds.), *Geologia e Recursos Minerais do Estado do Pará:* Sistema de Informações Geográficas - SIG: texto explicativo dos mapas Geológico e Tectônico e de Recursos Minerais do Estado do Pará. Escala 1:1.000.000. Belém, Companhia de Pesquisas de Recursos Minerais – CPRM, p. 39-112. Disponível em: <http://www.cprm.gov.br/publique/Geologia/Geologia-Basica/Cartografia-Geologica-Regional-624.html>. Accessed on: Sept, 2019.

Williams I.S. 1998. U-Th-Pb geochronology by ion microprobe. *In*: McKibben M.A., Shanks I., Ridley W.C.P., Ridley W.I. (Eds.), *Application of Microanalytical Techniques to Understanding Mineralizing Process*. El Paso: Society of Economic Geologists, Reviews in Economic Geology, 7, p. 1-35. https://doi.org/10.5382/Rev.07